Materials Letters 357 (2024) 135699

Contents lists available at ScienceDirect

Materials Letters

journal homepage: www.elsevier.com/locate/matlet

Impact of the temperature on the conductive filament morphology in HfO_2-based RRAM

Guillermo Vinuesa [a,*], Héctor García [a], Samuel Poblador [b], Mireia B. González [b], Francesca Campabadal [b], Helena Castán [a], Salvador Dueñas [a]

[a] Departamento de Electricidad y Electrónica, University of Valladolid, Paseo de Belén 15, 47011 Valladolid, Spain
[b] Institut de Microelectrònica de Barcelona, IMB-CNM (CSIC), Campus UAB, 08193 Barcelona, Spain

ARTICLE INFO

Keywords:
Resistive switching
Conductive filament
Schottky emission
Hopping
Temperature dependence

ABSTRACT

In this letter, we study the impact of the temperature on the resistive switching effect of TiN/Ti/HfO_2/W metal–insulator-metal devices. An analysis of the conduction mechanisms is made, with the low resistance state being ruled by nearest neighbor hopping, while the conduction in the high resistance state is dominated by Schottky emission. Taking into account the filamentary mechanism behind the resistive switching effect, a thorough analysis of the Schottky emission allows for the calculation of the gap between conductive filament tip and metal electrode in the high resistance state. We report an increase of this gap when temperature lowers below a certain value. Moreover, the mentioned gap adopts values of integer multiples of the the mean distance between traps obtained by the hopping model.

1. Introduction

In recent years, resistive random-access memories (RRAMs) based on the resistive switching (RS) effect have been extensively studied. Their characteristics (non-volatility, fast switching, low power consumption) are very appropriate for digital storage, neuromorphic circuits, or hardware cryptography [1–3]. The RS effect takes place when an electric field is applied to the opposite electrodes of a metal–insulator-metal (MIM) cell. Firstly, a conductive filament (CF) that short-circuits the metal electrodes through the dielectric is formed for the first time (electroforming). After the electroforming, the device reaches the low resistance state or LRS. Then, the CF can be partially ruptured creating a gap between the CF tip and the metal electrode, reaching a high resistance state or HRS (reset). The filament can then be formed again to return to the LRS (set) [4]. If no electrochemically active metal is used as electrode, the CF is formed by oxygen vacancies [5,6].

The impact of the temperature on both resistance states allows us to analyze their main conduction mechanisms. Previous RS temperature measurements on HfO_x-based devices report a wide variety of results [7]. Temperature-dependent conduction mechanisms reported for the HRS include quantum point contact (QPC) [8], space-charge-limited-conduction (SCLC) [9], Poole-Frenkel (P-F) [10] and Schottky emission (SE) [11,12]. While the LRS is usually ruled by ohmic [12] or hopping [13,14] conduction. Previous works have already stated that, when using Schottky emission as a model for the HRS, the dielectric thickness calculated is an effective thickness (d_{sw}) [11,12], that is, the gap between conductive filament tip and metal electrode in the high resistance state. Syu et al. [12] observed a relationship between resistance value and d_{sw}. In this work, we extend the scope by exploring the RS temperature dependence of TiN/Ti/HfO_2/W devices, analysing the conduction mechanisms in both resistance states. We focus on the HRS and use the Schottky emission model to study the impact of the temperature on d_{sw}.

2. Device fabrication and characterization

TiN/Ti/HfO_2/W devices were fabricated on 100 mm Si wafers, with a 500 nm SiO_2 layer grown by thermal oxidation to isolate the MIM devices from the Si wafer. Both top (TE) and bottom (BE) metal electrodes were deposited by magnetron sputtering, and are composed by a 200 nm TiN layer over a 15 nm Ti layer, and a 100 nm W layer, respectively. The 10 nm HfO_2 insulating film was deposited by Atomic Layer Deposition (ALD) at 225 °C using TDMAH and H_2O as precursors, while N_2 was used as carrier and purge gas. The measured devices (Fig. 1 (a-b)) have an area of 2.5 × 2.5 μm^2.

The electrical characterization was carried out in the 200–296 K

* Corresponding author.
E-mail address: guillermo.vinuesa@uva.es (G. Vinuesa).

https://doi.org/10.1016/j.matlet.2023.135699
Received 27 September 2023; Received in revised form 10 November 2023; Accepted 4 December 2023
Available online 10 December 2023
0167-577X/© 2024 The Authors. Published by Elsevier B.V. This is an open access article under the CC BY license (http://creativecommons.org/licenses/by/4.0/).

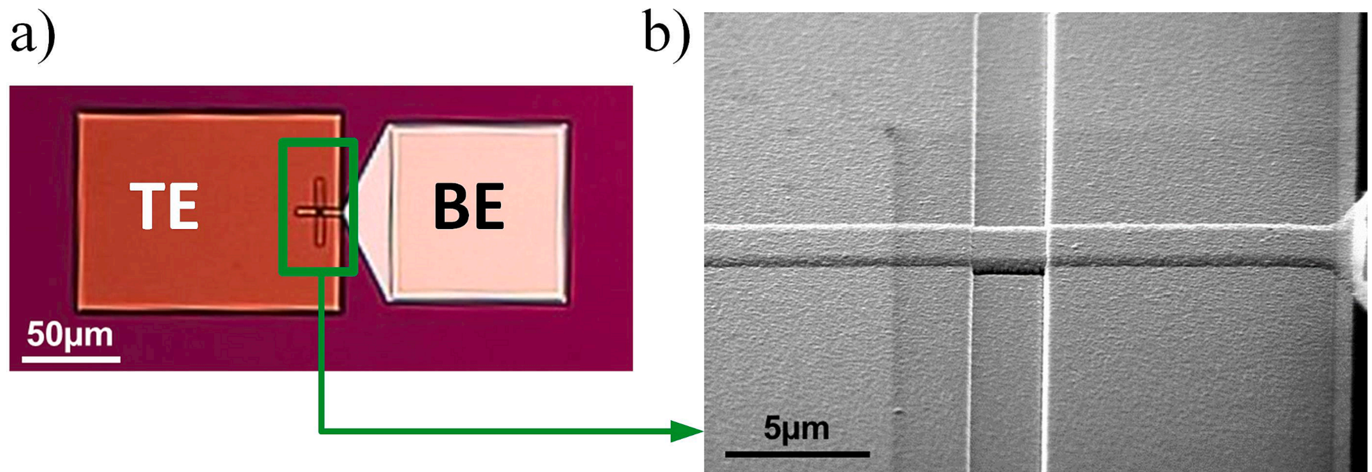

Fig. 1. (a) Optical microscope image of the MIM device. (b) SEM inspection.

temperature range by using an Oxford Instruments DM1710 cryostat and a Hewlett-Packard 4155B semiconductor parameter analyzer. The device was cooled with liquid nitrogen. Voltage bias was always applied to the TE with the BE grounded.

3. Results and discussion

After the electroforming process, TiN/Ti/HfO_2/W memory devices were cooled from 296 K to 200 K, measuring 20 I-V cycles every 20 K (see average cycles for each temperature on Fig. 2 (a)). There is a clear increase in set voltages as temperature decreases (Fig. 2 (b)), which can be related to the reduction of the thermal energies of oxygen vacancies [13,14], that need a stronger electric field to form the CF. This could significantly affect the performance of the samples when used in low-temperature applications [15].

Taking the cycle-to-cycle variability into account, the resistance increases for both states as the temperature lowers (Fig. 2 (c)). In the LRS, both the increase of the current with the applied voltage (Fig. 2 (d)) and the temperature dependence following the Arrhenius law (Fig. 2 (e)) can be effectively modelled by the hopping conduction mechanism, which occurs when trapped electrons "hop" to the nearest trap site through tunnelling effect. This mechanism is described by the following equation [16]:

$$I = qANv_0\exp\left(\frac{qaV}{2dk_BT} - \frac{\Phi_T}{k_BT}\right) \quad (1)$$

with q being the electron charge, A the area, N the density of space charge, a the mean distance between trap sites, v_0 the intrinsic frequency, k_B the Boltzmann constant, d the dielectric thickness and Φ_T the barrier height of hopping. The slope of the Arrhenius law on Fig. 2 (e) allows us to obtain the activation energy $\left(E_a = \Phi_T - \frac{qaV}{2d}\right)$ for several applied voltages. Representing E_a vs. the voltage (Fig. 2 (f)), the slope of the linear fit results in $a \sim 0.4nm$, similar to the average hopping distance reported by other authors [13,16].

In the HRS, our analysis focuses on the voltage range previous to the set process. As it can be seen in Fig. 3 (a - b), the HRS current values follow a linear fit for $\left(ln\left(\frac{I}{T^2}\right)vs.\sqrt{V}\right)$ and $\left(ln\left(\frac{I}{T^2}\right)vs.\frac{1}{k_BT}\right)$. Thus, the Schottky emission model effectively describes the main conduction mechanism in the HRS. The temperature dependence ruled out any tunneling mechanisms, which was further confirmed by the $\left(ln\left(\frac{I}{V^2}\right)vs.V^{-1}\right)$ linear fit in Fig. 3 (c), as it should have a negative slope to indicate Fowler-Nordheim tunneling. Schottky emission happens when thermally-activated electrons are injected over the energy barrier into the conduction band of the oxide, and is described by the following equation [7,11]:

$$I = AA^*T^2\exp\left(\frac{\sqrt{\frac{q^3V}{4\pi\epsilon d}}}{k_BT} - \frac{\Phi_{SE}}{k_BT}\right) \quad (2)$$

where A^* is the Richardson's constant, ϵ is the dielectric permittivity of the active layer and Φ_{SE} is the Schottky barrier height. If we consider the filamentary nature of the RS, it must be noted that d is not the dielectric thickness, rather, it is the gap between the partially ruptured CF tip and the metal [11,12], an effective thickness d_{sw}.

From the linear fitting of $\left(ln\left(\frac{I}{T^2}\right)vs.\sqrt{V}\right)$ in the previous equation, we can define the slope as $m = \frac{1}{k_BT}\sqrt{\frac{q^3}{4\pi\epsilon d_{sw}}}$. From these slope values delivered by the linear fits shown in Fig. 3 (a), we obtain thickness values smaller than the dielectric layer (and similar to those in [11,12]). When plotting these values against the temperature (Fig. 3 (d)), we can see that, in the 260–296 K range, d_{sw} remains almost constant. However, when the temperature drops below 260 K, the gap increases, reaching a value of $\sim 2.35nm$ at 200 K (Fig. 3 (d-e)). This is in good agreement with the increase in set voltages at low temperatures (Fig. 2 (b)). The decrease in HRS currents as temperature lowers indicates the increase in effective thickness, which ultimately results in higher voltage values to complete the set process. Moreover, the d_{sw} values are, approximately, integer multiples of the mean hopping distance (Fig. 3 (d)), which implies that the gap between CF tip and metal electrode in the HRS may only adopt discrete values defined by $d_{sw} = na, n \in \mathbb{N}$ (Fig. 3 (d-e)), with the lowest possible value being $d_{sw} = 3a$. This can be explained by the fact that the CF is formed by oxygen vacancies [5,6].

4. Conclusion

TiN/Ti/HfO_2/W devices show resistive switching characteristics in the 200–296 K temperature range. The hopping mechanism dominates the low resistance state. Meanwhile, the high resistance state is ruled by Schottky emission. Below a certain temperature, an increase in the gap between CF tip and metal electrode in the HRS is reported, which could account for the increase in set voltage at low temperatures. Furthermore, this gap adopts an integer value of the calculated mean hopping distance.

CRediT authorship contribution statement

Guillermo Vinuesa: Investigation, Conceptualization,

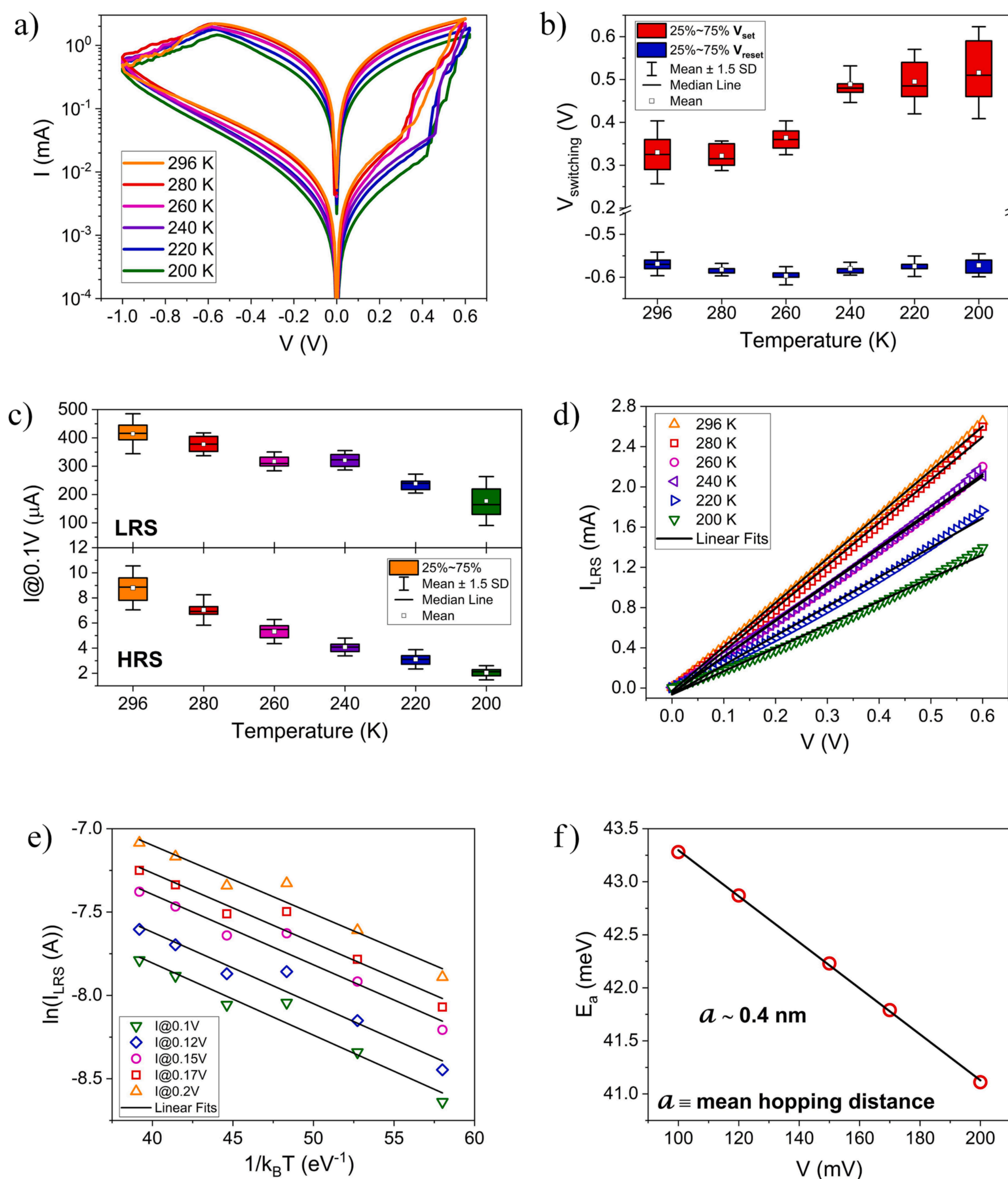

Fig. 2. (a) Average I-V curves of 20 cycles and (b) set and reset voltages at every temperature. (c) Current values measured at 0.1 V for both resistance states. (d – e) Hopping plots against voltage and temperature, respectively. (f) Activation energy vs. voltage.

Methodology, Validation, Formal analysis, Writing – original draft, Visualization, Writing – review & editing. **Héctor García:** Investigation, Methodology, Validation, Software, Writing – review & editing. **Samuel Poblador:** Investigation, Conceptualization. **Mireia B. González:** Investigation, Resources, Funding acquisition, Visualization, Project administration, Writing – review & editing. **Francesca Campabadal:** Resources, Funding acquisition, Project administration, Writing – review & editing. **Helena Castán:** Resources, Funding acquisition, Supervision, Project administration, Writing – review & editing. **Salvador Dueñas:** Resources, Funding acquisition, Supervision, Project administration, Writing – review & editing.

Declaration of Competing Interest

The authors declare that they have no known competing financial interests or personal relationships that could have appeared to influence the work reported in this paper.

Data availability

Data will be made available on request.

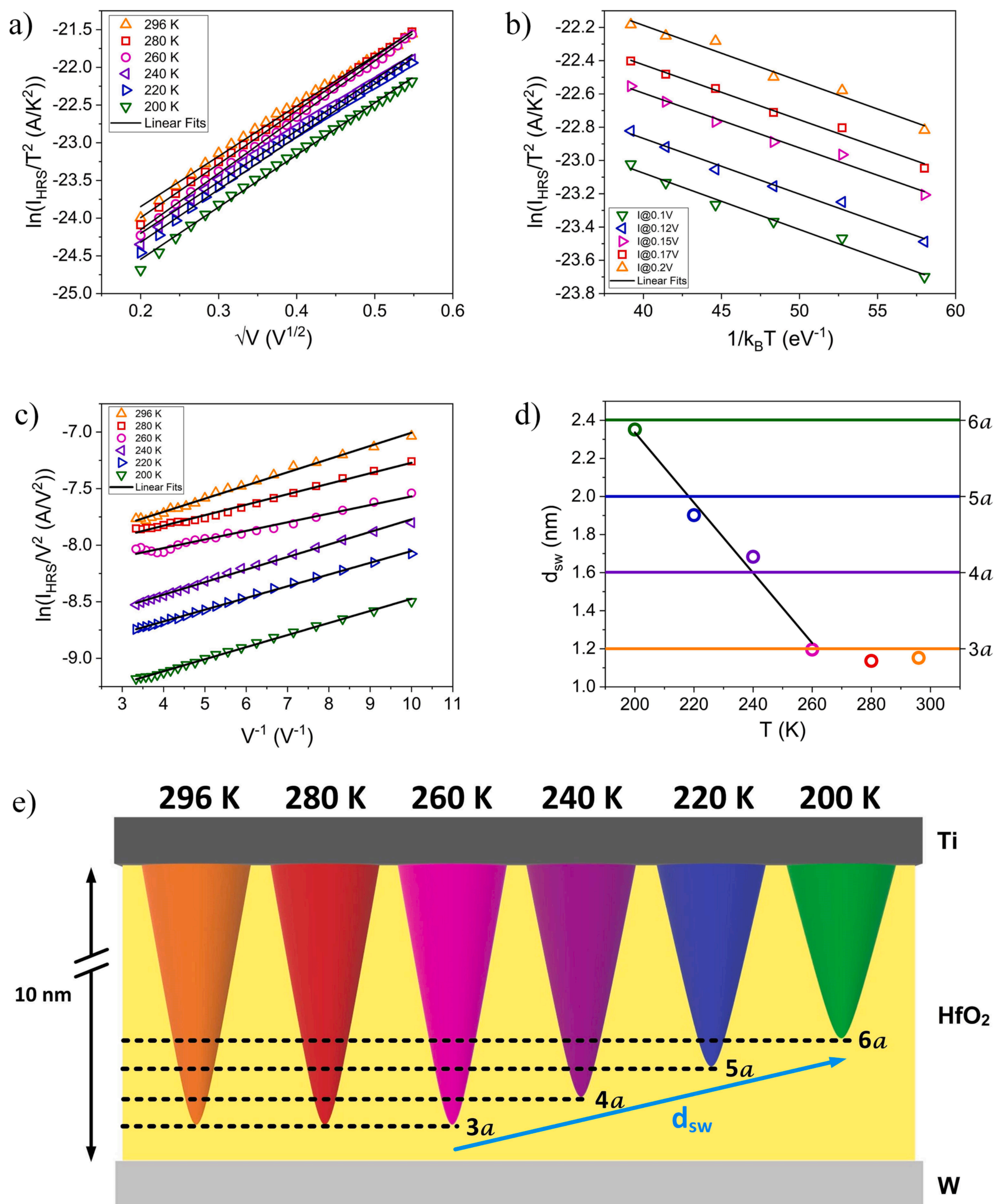

Fig. 3. (a-b) Schottky emission plots against voltage and temperature, respectively. (c) $\left(ln\left(\frac{I}{V^2}\right)vs.\frac{1}{V}\right)$ curves. (d) Effective thickness (d_{sw}) vs. temperature. (e) Visualization of the d_{sw} dependence with temperature (NOT TO SCALE).

Acknowledgements

This work was supported by the Spanish Ministry of Science (PID2022-139586NB-C42 and PID2022-139586NB-C43) and the Consejo Superior de Investigaciones Científicas (2022AT012). M.B. González acknowledges the Ramón y Cajal grant No. RYC2020-030150-I.

References

[1] F. Zahoor, T.Z. Azni Zulkifli, F.A. Khanday, Resistive random access memory (RRAM): an overview of materials, switching mechanism, performance, multilevel cell (mlc) storage, modeling, and applications, Nanoscale Res. Lett. 15 (90) (2020), https://doi.org/10.1186/s11671-020-03299-9.

[2] D. Ielmini, S. Ambrogio, Emerging neuromorphic devices, Nanotechnology 31 (9) (2020), https://doi.org/10.1088/1361-6528/ab554b.

[3] R. Khan, N. Ilyas, M.Z.M. Shamim, et al., Oxide-based resistive switching-based devices: fabrication, influence parameters and applications, J. Mater. Chem. C 9 (44) (2021) 15755–15788, https://doi.org/10.1039/D1TC03420K.

[4] A.C. Jasmin, Filamentary model in resistive switching materials, AIP Conf. Proc. 1901 (2017), 060004, https://doi.org/10.1063/1.5010507.

[5] Z.H. Wang, Q.H. Zhang, G. Gregori, et al., Control of charge order melting through local memristive migration of oxygen vacancies, Phys. Rev. Materials 2 (2018), 054412, https://doi.org/10.1103/PhysRevMaterials.2.054412.

[6] G. Di Martino, A. Demetriadou, W. Li, et al., Real-time in situ optical tracking of oxygen vacancy migration in memristors, Nat. Electron. 3 (2020) 687–693, https://doi.org/10.1038/s41928-020-00478-5.

[7] E.W. Lim, R. Ismail, Conduction mechanism of valence change resistive switching memory: a survey, Electronics 4 (2015) 586–613, https://doi.org/10.3390/electronics4030586.

[8] L.M. Prócel, L. Trojman, et al., Experimental evidence of the quantum point contact theory in the conduction mechanism of bipolar HfO2-based resistive random access memories, J. Appl. Phys. 114 (2013), 074509, https://doi.org/10.1063/1.4818499.

[9] H.Y. Lee, Y.S. Chen, P.S. Chen, et al., Low-power and nanosecond switching in robust hafnium oxide resistive memory with a thin Ti cap, IEEE Electron Device Lett. 31 (1) (2010) 44–46, https://doi.org/10.1109/LED.2009.2034670.

[10] C. Walczyk, D. Walczyk, T. Schroeder, et al., Impact of temperature on the resistive switching behavior of embedded HfO_2 -based RRAM devices, IEEE Trans. Electron Devices 58 (9) (2011) 43124–43131, https://doi.org/10.1109/TED.2011.2160265.

[11] O.O. Permiakova, A.E. Rogozhin, A.V. Miakonkikh, et al., Transition between resistive switching modes in asymmetric HfO2-based structures, Microelectron. Eng. 275 (2023), 111983, https://doi.org/10.1016/j.mee.2023.111983P.

[12] Y.-E. Syu, T.-C. Chang, J.-H. Lou, et al., Atomic-level quantized reaction of HfOx memristor, Appl. Phys. Lett. 102 (17) (2013), 172903, https://doi.org/10.1063/1.4802821.

[13] H. García, J. Boo, G. Vinuesa, et al., Influences of the temperature on the electrical properties of HfO2-based resistive switching devices, Electronics 10 (22) (2021) 2816, https://doi.org/10.3390/electronics10222816.

[14] R. Fang, W. Chen, L. Gao, et al., Low-temperature characteristics of hfo_x-based resistive random access memory, IEEE Electron Device Lett. 36 (6) (2015) 567–569, https://doi.org/10.1109/LED.2015.2420665.

[15] J.R. Rani, N.C. Das, M. Kim, et al., Low-temperature characteristics of resistive switching memory devices based on reduced graphene oxide-phosphor composites toward reliable cryogenic electronic devices, Carbon 195 (2022) 174–182, https://doi.org/10.1016/j.carbon.2022.04.016.

[16] K.-H. Chen, R. Zhang, T.-C. Chang, et al., Hopping conduction distance dependent activation energy characteristics of Zn:SiO2 resistance random access memory devices, Appl. Phys. Lett. 102 (13) (2013), 133503, https://doi.org/10.1063/1.4799655.